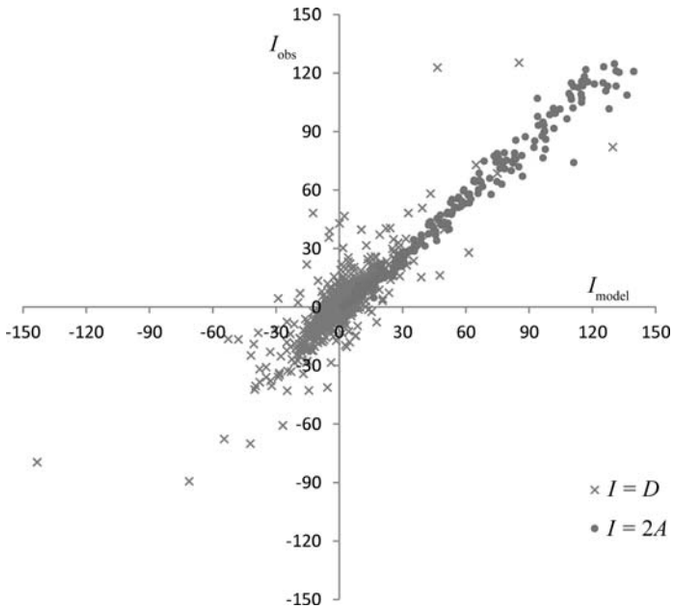

Figure 1.6.5.1
Data-evaluation plot for crystal Ex2. The plot shows a scattergram of all (D_{obs}, D_{model}) pairs and those ($2A_{obs}$, $2A_{model}$) pairs in the same intensity range as the D values.

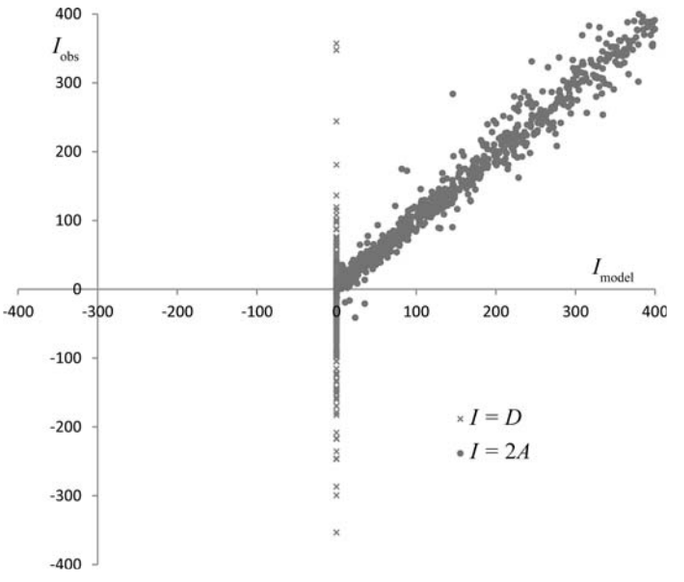

Figure 1.6.5.2
Data-evaluation plot for crystal Ex1. The plot shows a scattergram of all (D_{obs}, D_{model}) and some ($2A_{obs}$, $2A_{model}$) data points.

as 25% must be permitted in order to assemble an optimal set of operations to describe the diffraction symmetry. Another interesting procedure, accompanied by experimental proof, has been devised by Sauter *et al.* (2006). They show that it is clearer to calculate R_{merge} values individually for each potential symmetry operation of a target point group rather than comparing R_{merge} values for target point groups globally. According to Sauter *et al.* (2006) the reason for this improvement lies in the lack of intensity data relating some target symmetry operations.

The second characteristic of macromolecular crystals is that the compound is known, or presumed, to be chiral and enantiomerically pure, so that the crystal structure is chiral. This limits the choice of space group to the 65 Sohncke space groups containing only translations, pure rotations or screw rotations. For ease of use, these have been typeset in bold in Tables 1.6.4.2–1.6.4.30.

For the evaluation of protein structures, Poon *et al.* (2010) apply similar techniques to those described in Section 1.6.2.3. The major tactical objective is to identify pairs of α-helices that have been declared to be symmetry-independent in the structure solution but which may well be related by a rotational symmetry of the crystal structure. Poon *et al.* (2010) have been careful to test their methodology against generated structural data before proceeding to tests on real data. Their results indicate that some 2% of X-ray structures in the Protein Data Bank potentially fit in a higher-symmetry space group. Zwart *et al.* (2008) have studied the problems of under-assigned translational symmetry operations, suspected incorrect symmetry and twinned data with ambiguous space-group choices, and give illustrations of the uses of group–subgroup relations.

1.6.5.3. Space-group determination from powder diffraction

In powder diffraction, the reciprocal lattice is projected onto a single dimension. This projection gives rise to the major difficulty in interpreting powder-diffraction patterns. Reflections overlap each other either exactly, owing to the symmetry of the lattice metric, or approximately. This makes the extraction of the integrated intensities of individual Bragg reflections liable to error. Experimentally, the use of synchrotron radiation with its exceedingly fine and highly monochromatic beam has enabled considerable progress to be made over recent years. Other obstacles to the interpretation of powder-diffraction patterns, which occur at all stages of the analysis, are background interpretation, preferred orientation, pseudo-translational symmetry and impurity phases. These are general powder-diffraction problems and will not be treated at all in the current chapter. The reader should consult David *et al.* (2002) and David & Shankland (2008) or the forthcoming new volume of *International Tables for Crystallography* (Volume H, *Powder Diffraction*) for further information.

It goes without saying that the main use of the powder method is in structural studies of compounds for which single crystals cannot be grown.

Let us start by running through the three stages of extraction of symmetry information from the diffraction pattern described in Section 1.6.2.1 to see how they apply to powder diffraction.

(1) Stage 1 concerns the determination of the Bravais lattice from the experimentally determined cell dimensions. As such, this process is identical to that described in Section 1.6.2.1. The obstacle, arising from peak overlap, is the initial indexing of the powder pattern and the determination of a unit cell, see David *et al.* (2002) and David & Shankland (2008).

(2) Stage 2 concerns the determination of the point-group symmetry of the intensities of the Bragg reflections. As a preparation to stages 2 and 3, the integrated Bragg intensities have to be extracted from the powder-diffraction pattern by one of the commonly used profile analysis techniques [see David *et al.* (2002) and David & Shankland (2008)]. The intensities of severely overlapped reflections are subject to error. Moreover, the exact overlap of reflections owing to the symmetry of the lattice metric makes it impossible to distinguish between high- and low-symmetry Laue groups in the same family *e.g.* between 4/*m* and 4/*mmm* in the tetragonal family and $m\bar{3}$ and $m\bar{3}m$ in the cubic family. Likewise,

differences in intensity between Friedel opposites, *hkl* and $\overline{hkl}$, are hidden in a powder-diffraction pattern and the techniques of Section 1.6.5.1 are inapplicable. It is also known that experimental results on structure-factor statistics described in Section 1.6.2.2 are sensitive to the algorithm used to extract the integrated Bragg intensities from the powder-diffraction pattern. One procedure tends to produce intensity statistics typical of the noncentrosymmetric space group $P1$ and another those of the centrosymmetric space group $P\overline{1}$. In all, nothing much can be learnt from stage 2 for a powder-diffraction pattern. As a consequence, space-group determination from powder diffraction relies entirely on the Bravais lattice derived from the indexing of the diffraction pattern in stage 1 and the detection of systematic absences in stage 3.

(3) Stage 3 concerns the identification of the conditions for possible systematic absences. However, Bragg-peak overlap causes difficulties with determining systematic absences. For powder-diffraction peaks at small values of $\sin\theta/\lambda$, the problem is rarely severe, even for low-resolution laboratory powder-diffraction data. Potentially absent reflections at higher values of $\sin\theta/\lambda$ often overlap with other reflections of observable intensity. Accordingly, conclusions about the presence of space-group symmetry operations are generally drawn on the basis of a very small number of clear intensity observations. Observing lattice-centring absences is usually relatively easy. In the case of molecular organic materials, considerable help in space-group selection comes from the well known frequency distribution of space groups, where some 80% of compounds crystallize in one of the following: $P2_1/c$, $P\overline{1}$, $P2_12_12_1$, $P2_1$ and $C2/c$. Practical methods of proceeding are described by David & Sivia (2002). It should also be pointed out that Table 1.6.4.1 in this chapter may often be found to be helpful. For example, if it is known that the Bravais lattice is of type *cP*, Table 1.6.4.1 tells us that the possible Laue classes are $m\overline{3}$ and $m\overline{3}m$ and the possible space groups can be found in Tables 1.6.4.25 and 1.6.4.26, respectively. The appropriate reflection conditions are of course given in these tables. All relevant tables can thus be located with the aid of Table 1.6.4.1 if the Bravais lattice is known.

There has been considerable progress since 2000 in the automated extraction by software of the set of conditions for reflections from a powder-diffraction pattern for undertaking stage 3 above. Once the conditions have been identified, Tables 1.6.4.2–1.6.4.30 are used to identify the corresponding space groups. The output of such software consists of a ranked list of complete sets of conditions for reflections (*i.e.* the horizontal rows of conditions given in Tables 1.6.4.2–1.6.4.30). Accordingly, the best-ranked set of conditions is at the top of the list followed by others in decreasing order of appropriateness. The list thus is answering the question: Which is the most probable set of reflection conditions for the data to hand? Such software uses integrated intensities of Bragg reflections extracted from the powder pattern and, as mentioned above, the results are sensitive to the particular profile integration procedure used. Moreover, only ideal Wilson (1949) p.d.f.'s for space groups $P1$ and $P\overline{1}$ are implemented. The art of such techniques is to find appropriate criteria such that the most likely set of reflection conditions is clearly discriminated from any others. Altomare *et al.* (Altomare, Caliandro, Camalli, Cuocci, da Silva *et al.*, 2004; Altomare, Caliandro, Camalli, Cuocci, Giacovazzo *et al.*, 2004; Altomare *et al.*, 2005, 2007, 2009) have used a probabilistic approach combining the probabilities of individual symmetry operations of candidate space groups. The approach is pragmatic and has evolved over several versions of the software. Experience has accumulated through use of the procedure and the discrimination of the software has consequently improved. Markvardsen *et al.* (2001, 2012) commence with an in-depth probabilistic analysis using the concepts of Bayesian statistics which was demonstrated on a few test structures. Later, Markvardsen *et al.* (2008) made software generally available for their approach. Vallcorba *et al.* (2012) have also produced software for space-group determination, but give little information on their algorithm.

1.6.6. Space groups for nanocrystals by electron microscopy

By J. C. H. Spence

The determination of crystal space groups may be achieved by the method of convergent-beam electron microdiffraction (CBED) using a modern transmission electron microscope (TEM). A detailed description of the CBED technique is given by Tanaka (2008) in Section 2.5.3 of Volume B; here we give a brief overview of the capabilities of the method for space-group determination, for completeness. A TEM beam focused to nanometre dimensions allows study of nanocrystals, while identification of noncentrosymmetric crystals is straightforward, as a result of the strong multiple scattering normally present in electron diffraction. (Unlike single scattering, this does not impose inversion symmetry on diffraction patterns, but preserves the symmetry of the sample and its boundaries.) CBED patterns also allow direct determination of screw and glide space-group elements, which produce characteristic absences, despite the presence of multiple scattering, in certain orientations. These absences, which remain for all sample thicknesses and beam energies, may be shown to occur as a result of an elegant cancellation theorem along symmetry-related multiple-scattering paths (Gjønnes & Moodie, 1965). Using all of the above information, most of the 230 space groups can be distinguished by CBED. The remaining more difficult cases (such as space groups that differ only in the location of their symmetry elements) are discussed in Spence & Lynch (1982), Eades (1988), and Saitoh *et al.* (2001). Enantiomorphic pairs require detailed atomistic simulations based on a model, as in the case of quartz (Goodman & Secomb, 1977). Multiple scattering renders Bragg intensities sensitive to structure-factor phases in noncentrosymmetric structures, allowing these to be measured with a tenth of a degree accuracy (Zuo *et al.*, 1993). Unlike X-ray diffraction, electron diffraction is very sensitive to ionicity and bonding effects, especially at low angles, allowing extinction-free charge-density mapping with high accuracy (Zuo, 2004; Zuo *et al.*, 1999). Because of its sensitivity to strain, CBED may also be used to map out local phase transformations which cause space-group changes on the nanoscale (Zuo, 1993; Zhang *et al.*, 2006).

In simplest terms, a CBED pattern is formed by enlarging the incident beam divergence in the transmission diffraction geometry, as first demonstrated G. Mollenstedt in 1937 (Kossel & Mollenstedt, 1942). Bragg spots are then enlarged into discs, and the intensity variation within these discs is studied, in addition to that of the entire pattern, in the CBED method. The intensity variation within a disc displays a complete rocking curve in each of the many diffracted orders, which are simultaneously excited